Soft Matter

PAPER

View Article Online
View Journal | View Issue



Cite this: *Soft Matter*, 2025, **21**, 7476

# Comparison of acid- and base-catalysed sol–gel synthesis for the *in situ* crystallisation of a perovskite

Yutong Shen, [a] John D. Worth [ab] and Simon R. Hall *[a]

Received 13th June 2025,
Accepted 27th August 2025

DOI: 10.1039/d5sm00608b

rsc.li/soft-matter-journal

Confinement of ionic liquids (ILs) within solid matrices *via* sol–gel methods has been extensively studied to develop novel materials that retain the unique properties of the ionic liquids. In this study, the acid- and base-catalysed sol–gel synthesis of tetraethyl orthosilicate (TEOS) gels incorporating four ionic liquids: 1-butyl-3-methylimidazolium tetrafluoroborate and hexafluorophosphate, and 1-hexyl-3-methylimidazolium tetrafluoroborate and hexafluorophosphate was investigated. The influence of different methods, including catalysts and molar ratio, on the appearance, morphology and porosity of synthesised ionic silica gels was explored, along with their practical utility to grow bismuth halide perovskites *via* counter-diffusion in the resulting ionic gels. Scanning electron microscopy (SEM), transmission electron microscopy (TEM) and nitrogen ($N_2$) gas sorption data showed that the acid-catalysed ionic gels showed a continuous three-dimensional (3D) network and contained a large number of micropores and mesopores ($\leq$20 nm in diameter), whereas the base-catalysed ionic gels consisted of weakly connected nanoparticles with large voids. Powder X-ray diffraction (PXRD) confirmed that crystal formation was observed in all acid-catalysed ionic gels, while no crystals were found in base-catalysed ionic gels. These findings suggest that gels with a continuous solid-phase structure are better suited for crystal growth.



## 1. Introduction

Ionic liquids (ILs) are an established class of salts that have attracted attention in various fields over the past few decades.[1,2] Being completely ionic, the unique structure and low coulombic interactions between bulky organic cations and anions endow ILs with low melting points, low vapour pressure, a wide electrochemical window and high stability.[1–10] These desirable properties in turn endow ILs with great potential in applications including electrochemistry, catalysis and even as templates for synthesising novel inorganic materials,[1,6,11] for instance, immobilising ILs in solid materials to fabricate ionic gels, also known as ionogels.[1,2,10]

Confining ILs through a sol–gel method in solid materials has been studied extensively due to the need for building novel materials that could preserve the unique properties of ILs.[2] The encapsulation of ILs within the pore structure of a gel confers the high conductivity of the IL to the gel, as well as better temperature resistance and lower toxicity. In turn, the solid gel network prevents the leakage of the IL, which makes this composite material desirable in solid state materials.[1,12] Ionogels are chemically diverse due to the wide range of potential cations and anions that can be brought together, which means a specific IL can be chosen for ionogel synthesis to design suitable materials for specific applications. Moreover, ILs can act both as a catalyst and a templating agent. An example of this is in the most widely employed ILs in a sol–gel process, the alkyl-imidazolium ($C_nMIm^+$) ILs, which can reduce the silica aggregation and improve interphase interactions to form homogeneous materials with tailored morphologies under mild conditions.[13] For both hydrolytic and non-hydrolytic sol–gel routes, ILs tend to promote the rate of hydrolysis reaction when forming ionogels and further accelerating the gelation process.[13,14]

The primary applications of such ionogels are currently focused on electroactivity-related fields, including solid-state batteries and fuel cells, as well as separating membranes and catalysts.[15] However, it is also believed that the favourable properties offered by ILs and ionogels, *e.g.*, durability and high chemical stability, could expand the array of applications to other fields, for instance, in the growth of crystals in ionogels by gel diffusion. The gel diffusion crystal growth method brings

[a] *School of Chemistry, University of Bristol, Cantock's Close, Bristol, BS8 1TS, UK. E-mail: simon.hall@bristol.ac.uk*
[b] *Bristol Composites Institute, University of Bristol, University Walk, Bristol, BS8 1TR, UK*

 

several important benefits over traditional methods: a stable reaction medium, free from convection and temperature changes, the transparency also allows for good observation of diffusion at all stages of crystal growth.[16] Previous studies have demonstrated successful crystal growth in hydrogels and organic gels and many high-quality mineral-related compounds and oxysalts can only be obtained in gel medium. Additionally, perovskite materials for photovoltaics could also be synthesised through gel diffusion. Selivanov *et al.* have successfully grown good quality methylammonium lead halide perovskite crystals through the counter diffusion-in-gel technique.[17] Moreover, according to the literature, most $A_3B_2X_9$ perovskites can be synthesised *via* solution processing methods, for instance, less toxic methylammonium bismuth iodide solids can be prepared by mixing MAI and $BiI_3$ solution, providing the possibility of growing high quality crystals in gel by adding solutions separately.[18]

Different sol–gel methods and catalysts can be used to synthesise ionogels. Typical materials used in the sol–gel method are silica alkoxides such as tetramethyl orthosilicate (TMOS) and tetraethyl orthosilicate (TEOS). Reaction of these sources of silica with acid to catalyse hydrolysis and condensation has long been a common method of manufacturing silica gels,[10] with acids such as $H_2SO_4$, HCl, and formic acid (FA) typically used.[19,20] Based on the work of Dai *et al.*, monolithic ionogels using alkyl-imidazolium and butyl-pyridine ILs can be formed through a non-hydrolytic sol–gel process with a FA catalyst.[21] While successful HCl catalysed hydrolytic sol–gel formation was reported by Shi *et al.*,[22] due to these pioneering works, numerous studies in acidic catalysis have been developed. In contrast to acid-catalysed sol–gel methods, base-catalysed approaches have received comparatively less attention in the literature. Previous works have reported using ammonia solution and amines such as diethanolamine and octylamine, but the synthesis of base catalysis ionogel formation is scarcely reported.[23] In contrast to acid-catalysed gels, according to the literature, uniform silica particles could be synthesised by hydrolysing silicon alkoxides in aqueous alcoholic solutions containing ammonia through the Stöber method.[19,23,24] Owing to the complexity of the silicon oxide system, a number of parameters, including temperature, pH and catalyst influence the structure and morphology of products, yet to the best of the author's knowledge, a systematic comparison between different catalysis on ionogels is still lacking.[25–27]

In the present work, several sets of silica ionogels were prepared from alkyl-imidazolium ILs with tetrafluoroborate and hexafluorophosphate anions using hydrochloric acid and ammonia solution as catalysts with TEOS. The two sol–gel methods (acid-catalysis and base-catalysis, respectively) were compared on the basis of (1) appearance, (2) morphology, (3) surface and porosity characteristics, and (4) practical utility in gel diffusion crystal growth of bismuth halide perovskites.

We report on the results which provide a systematic comparison between acid-catalysis and base-catalysis in silica ionogel formations.

# 2. Materials and methods

The materials and instrumental conditions applied in this work are described herein.

## 2.1. Materials

All chemicals and reagents were purchased from commercial suppliers and used as received.

Tetraethyl orthosilicate [TEOS, Sigma-Aldrich, 98%]; 1-methylimidazole [$C_4H_6N_2$, Thermo Scientific, 99%]; 1-bromobutane [$C_4H_9Br$, Sigma-Aldrich, 99%]; 1-bromohexane [$C_6H_{13}Br$, Thermo Scientific, 99%]; potassium hexaflurophosphate [$KPF_6$, Sigma-Aldrich, $\geq$99%]; potassium tetrafluoroborate [$KBF_4$, Thermo Scientific, 98%]; Celite [$SiO_2$, Thermo Scientific, filter aid, standard]; bismuth(III) oxide [$Bi_2O_3$, Sigma-Aldrich, 99.9%]; hydriodic acid [HI, Thermo Scientific, 57 wt% in $H_2O$]; ammonia solution [$NH_4OH$, Supelco, 25%]; polyethylene glycol MW = 400 [PEG400, Thermo Scientific, >99%]; ethanol [$C_2H_5OH$, Fisher Scientific, $\geq$99.8%]; dichloromethane [$CH_2Cl_2$, Fisher Scientific, $\geq$99%]; methylamine [$CH_3NH_2$, Sigma-Aldrich, 40% solution in water]; and hydrochloric acid [HCl, VWR Chemicals, 37%].

## 2.2. Synthetic procedures

Details concerning the synthesis of the investigated materials are given.

**2.2.1. Synthesis of imidazolium-based ionic liquids.** $C_4MImBF_4$ and $C_6MImBF_4$ ILs: 1-bromoalkane and 1-methylimidazolium were stirred and heated at 90 °C for 5 h. $KBF_4$ was added and stirred after the precursor was cooled, and acetonitrile was added to dissolve any residue. The molar ratio of bromoalkane : methylimidazolium : $KBF_4$ was 1 : 1 : 1. Vacuum filtration and rotary evaporation were used to remove unwanted product and solvent.

$C_4MImPF_6$ and $C_6MImPF_6$ ILs: 1-bromoalkane and 1-methylimidazolium were stirred and heated at 90 °C for 5 h. $KPF_6$ was added and stirred, after the precursor was cooled, distilled water was added to dissolve any residue. The molar ratio of bromoalkane : methylimidazolium : $KPF_6$ was 1 : 1 : 1. Dichloromethane-assisted layer separation and rotary evaporation were used to remove unwanted product and solvent.

**2.2.2. Synthesis of acid-catalysed TEOS ionogels.** The synthesis of acid-catalysed TEOS ionogels followed a modified version of the reported procedure by Shi *et al.*[22] Briefly, this involved 0.0448 mol (10 mL) of TEOS and 0.1200 mol (7 mL) of EtOH which were heated to 60 °C and stirred for 30 min by a magnetic stirrer in a sealed glass conical flask, 1 g of ILs being added quickly after. After stirring again for 5 min, 0.0303 mol of HCl (2.5 mL, conc. 37%) diluted with 3 mL distilled water was added and stirred for another 10 min. The solution was then allowed to cool to room temperature and transferred to a glass U-tube with a diameter of 15 mm. Precursors were left to change from viscous sols to gels under room temperature (20 °C) and atmosphere in a fume hood, the relative humidity is 41% (Schemes 1 and 2).

**2.2.3. Synthesis of base-catalysed TEOS ionogels.** The base catalysis method was adapted from Xiang *et al.*[28] EtOH

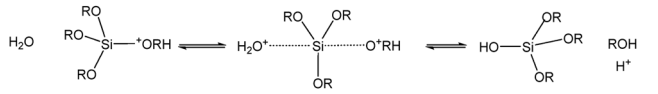

Scheme 1 Schematic showing the acid-catalysed hydrolysis reaction of TEOS, based on the reported procedure by Brinker *et al.*[20]

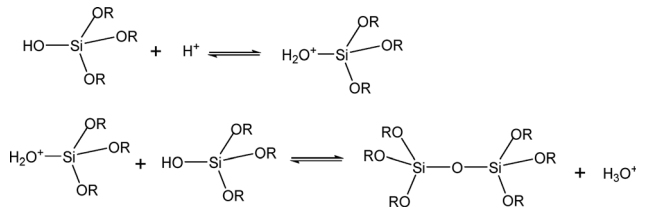

Scheme 2 Schematic showing the acid-catalysed condensation reaction of TEOS, based on the reported procedure by Brinker *et al.*[20]

(0.38 mol) and TEOS (0.01 mol) were stirred together at 500 rpm using a magnetic stirrer in a sealed glass conical flask on a hotplate for 30 min at room temperature (20 °C). $NH_3$ (5.40 mmol) and $H_2O$ (0.0151 mol) were then added and stirred at 500 rpm for a further 30 min at room temperature. Modifying agent PEG400 (0.51 mmol) and IL (1 g) were added to the precursor 24 h after the addition of base, and the mixture was then stirred at 500 rpm for another 30 min at room temperature. The molar ratio of TEOS : EtOH : $NH_3$ : $H_2O$ : PEG400 is 1 : 38 : 0.54 : 1.51 : 0.051 (the $H_2O$ is present in the ammonia solution). The precursors were transferred to U-shaped tubes with a diameter of 15 mm after mixing and were left to change from viscous sols to gels at room temperature and atmosphere in a fume hood, the relative humidity is 41% (Schemes 3 and 4).

**2.2.4. Double diffusion of $MA_3Bi_2I_9$ perovskite crystal growth.** $Bi_2O_3$ (0.0045 mol, 2.093 g) was dissolved in 10 mL of HI, while methylamine (0.0130 mol, 1.040 g) was mixed with HI (0.0130 mol, 1.050 g). The formed $BiI_3$ and MAI solutions were added to opposing sides of a U-tube to allow slow counter diffusion.

### 2.2. Characterisation

Methods of characterisation used and instrument details are given in this section.

**2.2.1. Microscopy.** Scanning electron microscopy (SEM) was used to image silver-coated gel samples, *via* a JEOL IT300 SEM. Transmission electron microscopy (TEM) was used to determine the exact microstructures *via* a JEOL JEM2100 TEM. Samples were refluxed in acetone at 60 °C for 4 h and dried in a furnace at 80 °C for 24 h before microscopy characterisation.

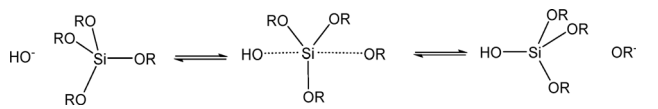

Scheme 3 Schematic showing the base catalysed hydrolysis reaction, based on the reported procedure by Brinker *et al.*[20]

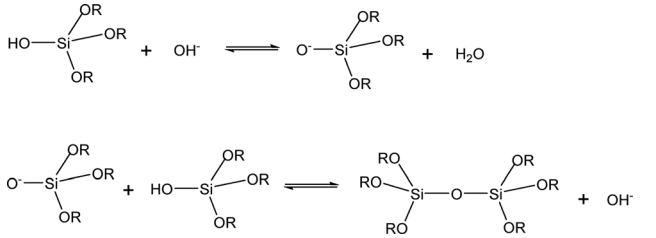

Scheme 4 Schematic showing the base catalysed condensation reaction, based on the reported procedure by Brinker *et al.*[20]

**2.2.2. Powder X-ray diffraction.** The phase of the formed crystals was characterised using powder X-ray diffraction (PXRD), recorded using CuK$\alpha$ radiation, $2\theta$ scan range 5–50°, step size 0.02° step$^{-1}$, at 2 s step$^{-1}$, using a Bruker D8 Advance powder X-ray diffractometer.

**2.2.3. Volumetric nitrogen gas sorption.** The porosity and surface characteristics of the materials were assessed using an Anton Paar NOVAtouch LX$^2$ gas sorption analyser for all samples. Before any analysis, approximately 0.070 g of the sample was subjected to a rigorous *in situ* degassing procedure (degas temperature was 573 K for Acid-1 and Acid-4 gels and 473 K for Base-1 and Base-4 gels). Nitrogen ($N_2$) isotherms were collected at 77 K within the range of relative pressures ($P/P_0$) $0.025 \leq P/P_0 \leq 1.0$. A thermal transpiration correction was applied to the collected isotherms. The specific surface area (SSA) of all samples were determined using the classical Brunauer–Emmett–Teller (BET) theory.[29] Classically calculated total pore volumes ($V_P$) were derived *via* the Gurvich method using an adsorption point at $P/P_0 \approx 0.95$. Differential pore size distributions (PSD), total pore volume ($V_{DFT}$), and an additional value for specific surface area for all samples were derived from the $N_2$ isotherms using a non-local density functional theory (NLDFT) kernel, assuming a cylindrical pore model on a silica surface with $N_2$ as the adsorbate at 77 K.[30]

## 3. Results and discussion

Experimental results and a discussion comparing the ionogels synthesised by the two methods (acid-catalysed and base-catalysed) are presented herein.

### 3.1. Results

Data from the experiments and characterisation are offered in this section.

**3.1.1. Sols and gelation.** Two series of ionogels were synthesised with four different ILs, butyl- and hexyl-imidazolium ILs with tetrafluoroborate $BF_4^-$ and hexafluorophosphate $PF_6^-$ anions. The sample name and materials used in each experiment are listed in Table 1.

In the acid-catalysis series, all four experiments formed transparent, hard and homogeneous gels from sols within 14 h as shown in Fig. 1a. The pH values of the four precursors were in the range 1.8–2.1 according to an EcoTestr pH meter. The gelation point was determined *via* the tilting method.

 

Table 1 Sample name, catalyst and ionic liquid used in each experiment

| Sample name | Catalyst | Ionic liquid |
|---|---|---|
| Acid-1 | HCl | $C_4MImBF_4$ |
| Acid-2 | HCl | $C_4MImPF_6$ |
| Acid-3 | HCl | $C_6MImBF_4$ |
| Acid-4 | HCl | $C_6MImPF_6$ |
| Base-1 | $NH_4OH$ | $C_4MImBF_4$ |
| Base-2 | $NH_4OH$ | $C_4MImPF_6$ |
| Base-3 | $NH_4OH$ | $C_6MImBF_4$ |
| Base-4 | $NH_4OH$ | $C_6MImPF_6$ |

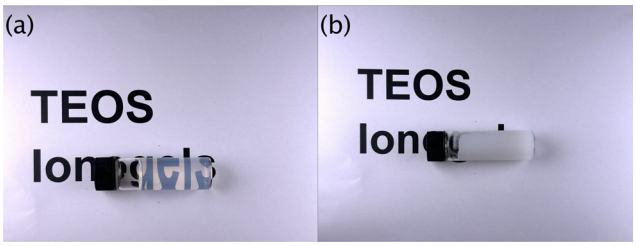


Fig. 1 Digital photographs to show (a) acid-catalysed ionogel Acid-1 and (b) base-catalysed ionogel Base-1. Texts used to highlight transparency.

Viscosity of sols continued to increase and eventually Acid-1 and Acid-3 gels completed gelation in 20 min, while Acid-2 and Acid-4 gels required 14 h to become fully gelled, which is consistent with data reported in previous literature.[1,2] Compared with the gelation time of pure silica gel following the same method, which took at least 2–3 days to form gels, the gelation time of ionogels was largely reduced in the presence of ILs. Although the formed ionogels were transparent and crack-free at first, cracks were found to be developed in several days after gelation. Circular cracks were observed inside the gel body, from which clear liquid emerged, which was identified as a mixture of ethanol and IL *via* proton nuclear magnetic resonance ($^1$H NMR) spectroscopy analysis as shown in Fig. S2 (SI).

Unlike acid-catalysed gels, base-catalysed gels were translucent, as shown in Fig. 1b, soft and easily penetrable, and the pH values of the precursor fell in the 10.3–10.5 range. The homogeneous base-catalysed gels were formed rapidly (within 10 min) after the addition of PEG400 and ILs. Like acid-catalysed gels, the addition of ILs into the precursor also accelerated the gelation process. According to existing literature and experimental data, the viscosity of the sols without addition of ILs remained the same after 12 h,[28] and completed gelation after 15 days.[23] These weak gels were able to move freely inside the containers, but the structure was very loose. The gels could break into small pieces easily, due to the weak crosslinking between silica particles, as described in the literature. Additionally, a clear liquid separated from the gel after gelation, which was also identified as a mixture of ethanol and ILs based on NMR analysis in Fig. S3 in the SI.

**3.1.2. Scanning electron microscopy.** SEM results reveal that HCl-catalysed TEOS gels possess stacked, irregular agglomerates and have a three-dimensional (3D) continuous structure

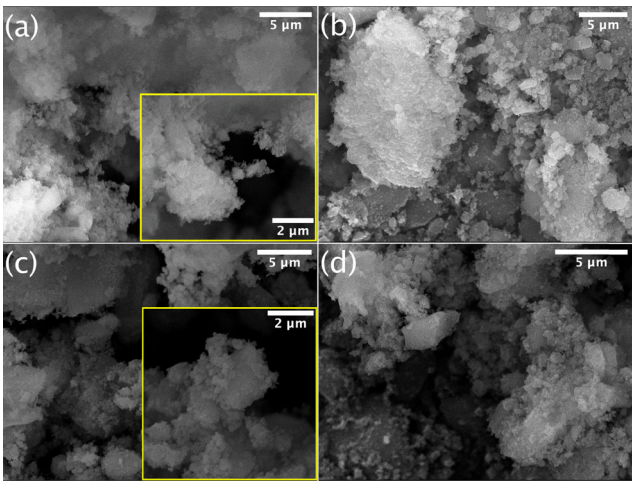


Fig. 2 SEM micrographs of (a) Acid-2 gel, (b) Acid-3 gel, (c) and (d) Acid-4 gel. Scale bars in all four images are 5 μm, insets with 2 μm scale bars have been added to selected images for greater detail.

(Fig. 2). Additionally, only a very small number of dark voids are visible on the surface (Fig. 2c), which may represent the small pore sizes contained in acid-catalysed gels. Previous literature has stated that, in strongly acidic environment (pH $<$ 3), the rapid hydrolysis of TEOS leads to the formation of small, highly branched polymers. These species then condense to create a microporous network with smaller pore sizes and large specific surface area. Previously, Faustova and Slizhov also reported the microporous silica gel prepared at pH = 2, containing micropores averaging 2 nm in diameter.[31]

The SEM results of base-catalysed ionogels show the formation of small silica nanoparticles during synthesis. These fine powders aggregated into irregular clusters of varying sizes with low degree of coalescence. Compared with the SEM results of the acid-catalysed gels, the dark spots observed in Fig. 3a–c were more obvious, showing the presence of larger voids and pores between the nanoparticles, confirming the porous nature of these materials, which is consistent with the literature.[23] Gels prepared in alkaline solution tend to form large silica nanoparticles that further aggregate to form spherical secondary particles.[20,23,28] Such a process involves continuous nucleation and growth through particle aggregation, subsequently resulting in uniform particle sizes and silica gel contains larger pores.[31]

**3.1.3. Transmission electron microscopy.** TEM analysis revealed that acid-catalysed gels appeared to have an interconnected mesoporous structure. The small void in acid-catalysed gels, as shown in squares in Fig. 4a, was approximately 2 nm in width and 5 nm in length, indicating the development of a porous structure. Additionally, neck formation between particles is observed in Fig. 4a, showing that the particles interconnect to form a linear arrangement under acid catalysis, which aligns with findings reported in the literature.[19] The structure shown in Fig. 4c consists of large condensed, irregularly shaped clusters of particles, further confirming that the silica gels formed the structure as described in previous studies.[19,32]

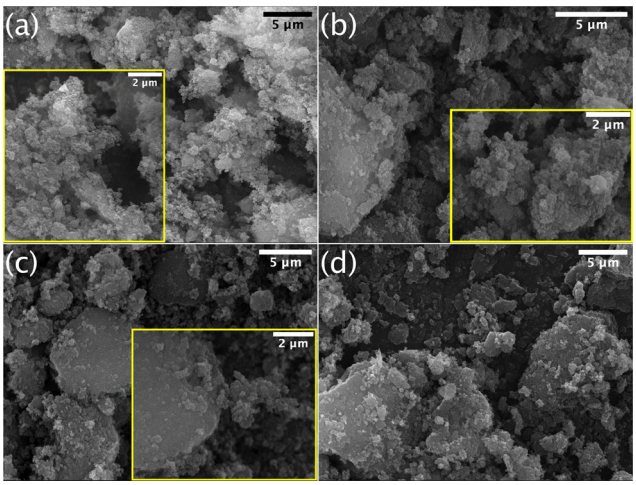


Fig. 3 SEM micrographs of (a) Base-1 gel, (b), (c) and (d) Base-4 gel. Scale bars in all four images are 5 μm, insets with 2 μm scale bars have been added to selected images for greater detail.

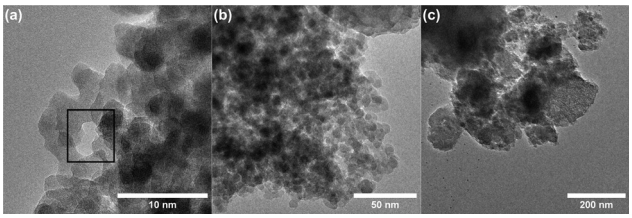


Fig. 4 TEM micrographs of Acid-1 gel. Scale bar in (a) is 10 nm, in (b) is 50 nm, and in (c) is 200 nm.

Compared to the TEM imagery of the acid-catalysed gels, base-catalysed gels exhibited hierarchical packing of well-defined visible spherical nanoparticles approximately 3–5 nm in size (Fig. 5a and c), similar to results in existing literature.[33] Fig. 5b shows a cluster of nanoparticles of similar sizes forming an aggregate. Unlike acid-catalysed gels, which showed relatively small pores, large voids ranging from 22–30 nm in diameter were observed between nanoparticles as shown in black rectangles in Fig. 5b and c. These voids likely represent the spaces between nanoparticle packing, which enable liquid percolation within the gel and therefore contribute to the faster diffusion of liquids than in acid-catalysed gels. The influence of PEG400 was not observed in the TEM results, as corroborated by Fourier-transform infrared (FTIR) spectroscopy (Fig. S1).

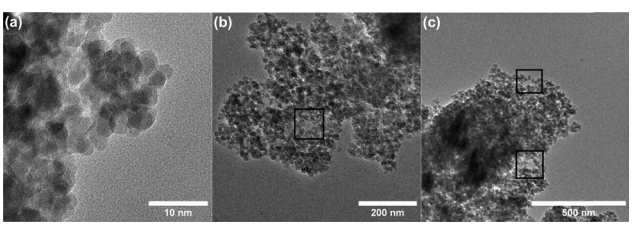


Fig. 5 TEM micrographs of Base-4 gel. Scale bar in (a) is 10 nm, in (b) is 200 nm, and in (c) is 500 nm.

Purification involved washing and heating the samples, thereby preserving only the solid silica network.

**3.1.4. Volumetric nitrogen gas sorption.** $N_2$ adsorption isotherms of both Acid-1 and Acid-4 samples are presented in Fig. 6. According to the classifications by the International Union of Pure and Applied Chemistry (IUPAC),[34] the Acid-1 sample exhibits a type I(b) isotherm, which is indicative of a material with a broad distribution of micropores (0–2 nm) and small mesopores (defined as pores 2–50 nm in diameter). The observed linear increase in $N_2$ adsorbed quality between $0.03 \leq P/P_0 \leq 0.5$ reflects the filling of these small diameter mesopores, and the subsequent plateau indicates that the pores become fully saturated. In contrast, Acid-4 shows a type IV(a) isotherm, characteristic of mesoporous adsorbents with larger diameter pores. The hysteresis observed is attributed to capillary condensation when the pore width exceeds a certain critical width, for $N_2$ adsorption in cylindrical pores at 77 K, hysteresis starts to occur for pores wider than $\approx$4 nm,[34] further confirmed the mesoporous nature of Acid-4 sample. The isotherm collected for Acid-4 sample showed the H2(b) hysteresis loop, attributed to the existence of pore cavities larger in diameter than the openings leading to them, so-called "ink-bottle" pores (a pore structure with a narrow neck and a wider body, which can hinder gas desorption due to delayed emptying of the wider cavity).[33]

Fig. 7 presents the pore size distribution results derived from the adsorption branch of the $N_2$ isotherms for both samples. The analysis reveals both microporosity and mesoporosity in the Acid-1 sample, with a predominant pore diameter of $\approx$4 nm, and no pores larger than 7 nm were observed, in agreement with the high specific surface area listed in Table 2. Gregg and Sing also reported that a specific surface area larger than $\approx$500 $m^2\ g^{-1}$ should be indicative that considerable microporosity may be presented.[35] In contrast, Fig. 7b

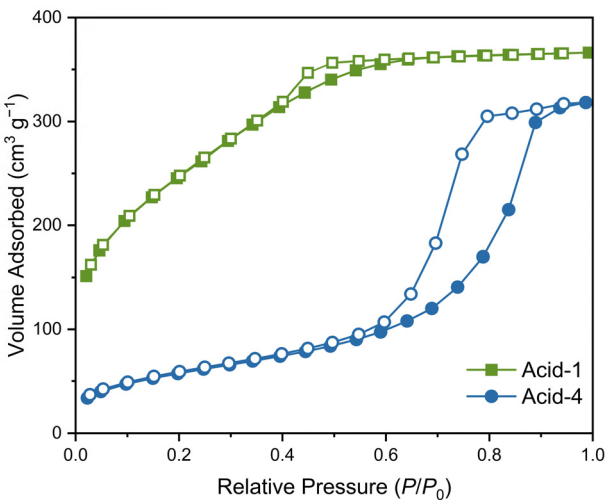


Fig. 6 Nitrogen adsorption and desorption isotherms of Acid-1 and Acid-4 samples collected at 77 K between $0.025 \leq P/P_0 \leq 1.0$. Adsorption branches are denoted by the filled symbols and desorption branches by the empty symbols.

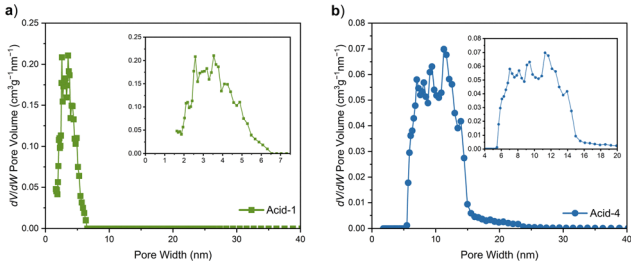


Fig. 7 Pore size distribution plots for (a) Acid-1 and (b) Acid-4 derived from the $N_2$ isotherms using an NLDFT kernel, assuming a cylindrical pore model on a silica surface with $N_2$ as the adsorbate at 77 K. The insets highlight the predominant pore sizes.

displays the broader pore size distribution obtained for Acid-4 sample, indicating the presence of mesopores predominantly in the lower mesopore range, with a modal pore diameter of around 12 nm. No pores exceed approximately 20 nm. Viau *et al.* suggested that the longer gel time observed with $PF_6^-$ anions was associated with this broad pore size distribution.[1] The results reveal that both samples have relatively small pores in structure, in agreement with the observation in SEM and TEM analyses and previous literature.[1,22,36]

Fig. 8 shows the $N_2$ adsorption isotherms for Base-1 and Base-4 gels. Similar to Acid-4 gel, Base-4 gel also exhibited a type IV(a) isotherm, which is indicative of the mesoporous nature of this material and the presence of ink-bottle pores in its structure.[32] In contrast, the Base-1 gel presents a type II isotherm with an H3 hysteresis loop, which is generally associated with nonporous or macroporous adsorbents, similar to findings reported by Framery and Mutin.[36] Both isotherms show lower volume adsorbed at intermediate relative pressures compared to the acid-catalysed gels, suggesting the reduced amount of smaller mesopores in the structure. The sharp increase at high relative pressure ($P/P_0 \approx 0.8$) indicates capillary condensation in larger mesopores or macropores.[32,35]

Fig. 9 presents the pore size distribution results of the two samples. In contrast to the results of acid-catalysed samples, base-catalysed gels tend to have broader pore size distribution, consistent with the increased adsorption at high relative pressures in the isotherms. The results indicate the absence of micropores in these samples. Instead, both contain a significant amount of mesopores with a diameter ranging from 15–30 nm, which corresponds to the lower specific surface area listed in Table 2. These results are in agreement with the observation of significant dark spots in SEM and large voids between nanoparticles in TEM, as well as the observed fast

Table 2 Summary of specific areas as determined by BET ($S_{BET}$) and NLDFT ($S_{DFT}$), and specific total pore volumes as determined classically ($V_P$) and by using NLDFT ($V_{DFT}$)

| Sample | $S_{BET}$ ($m^2\ g^{-1}$) | $S_{DFT}$ ($m^2\ g^{-1}$) | $V_P$ ($cm^3\ g^{-1}$) | $V_{DFT}$ ($cm^3\ g^{-1}$) |
|---|---|---|---|---|
| Acid-1 | 885 | 738 | 0.57 | 0.54 |
| Acid-4 | 209 | 195 | 0.49 | 0.48 |
| Base-1 | 176 | 149 | 0.36 | 0.58 |
| Base-4 | 163 | 169 | 0.54 | 0.74 |

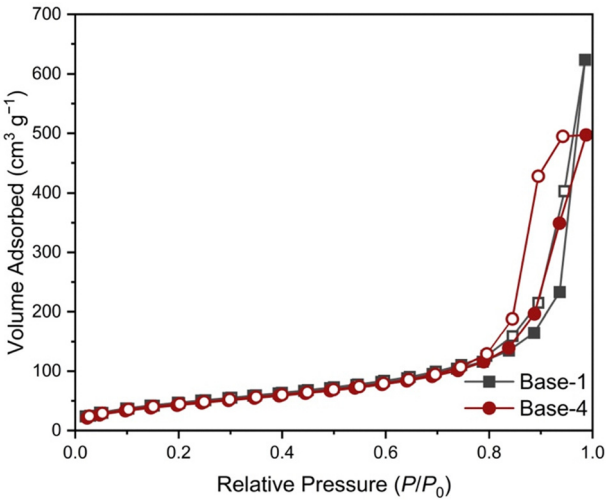


Fig. 8 Nitrogen adsorption isotherms of Base-1 and Base-4 samples collected at 77 K between $0.025 \leq P/P_0 \leq 1.0$. Adsorption branches are denoted by the filled symbols and desorption branches by the empty symbols.

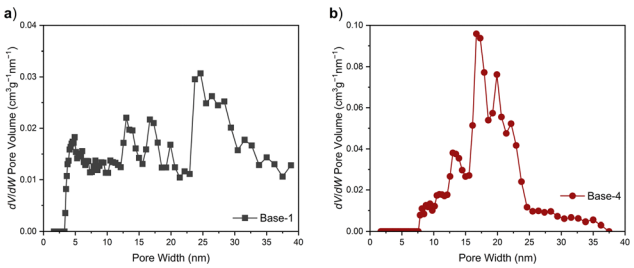


Fig. 9 Pore size distribution plots of (a) Base-1 and (b) Base-4 samples derived from the $N_2$ isotherms using an NLDFT kernel, assuming a cylindrical pore model on a silica surface with $N_2$ as the adsorbate at 77 K.

diffusion of liquids in these gels. The Base-1 sample exhibits the broadest pore size distribution, and based on the trend and the isotherm, it is reasonable to estimate that macropores may also be present in this gel.

**3.1.5. Behaviour in crystal growth.** When applying these ionogels in counter-diffusion crystal growth experiments, it was found that reagents in acid-catalysed ionogels diffused slowly inside U-shaped tubes. However, because of the cracks in the gel, liquids tended to diffuse through these cracks and eventually causing uneven diffusion. In those cases, fine powder and crystals were found to have grown inside these cracks.

Crystals were found to form successfully in all acid-catalysed ionogels. Most of the collected crystals were dark red and flaky with irregular shapes, consistent with the appearance described in literature.[37]

Apart from those crystals, polycrystalline red powder was also observed in the gels. Crystals obtained from experiments had typical diameters of between 2–5 mm as shown in Fig. S8. Moreover, instead of 3D solids, these crystals were flatter, which may be due to the growth environment, as the silica walls may restrict subsequent growth, as the gel body is too stiff

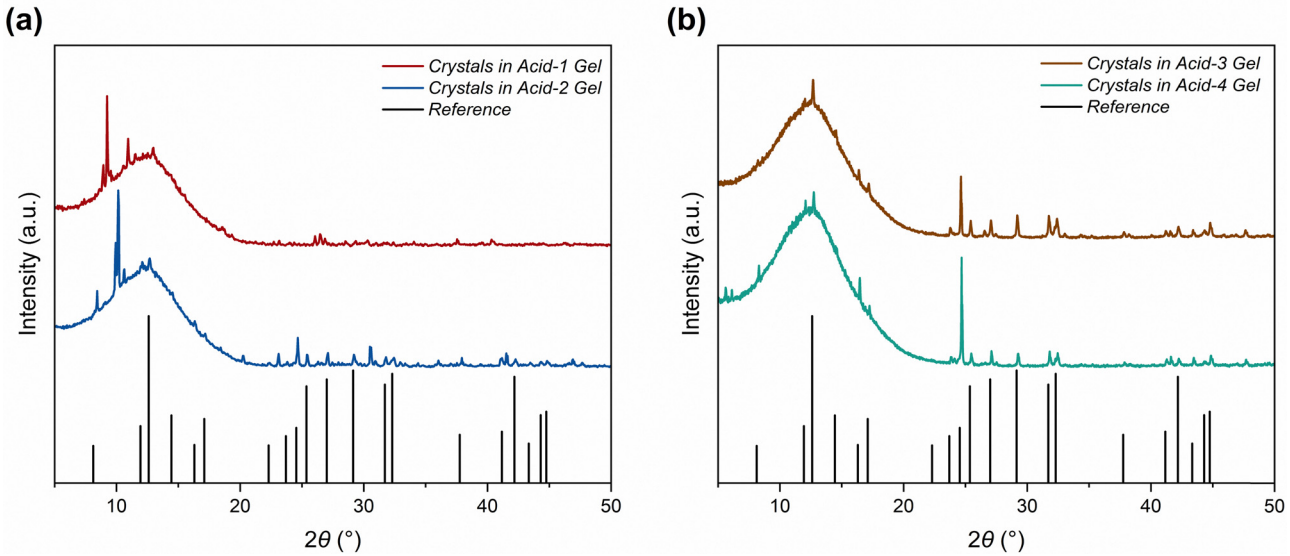


Fig. 10 PXRD patterns of (a) crystals grown in Acid-1 and Acid-2 gels; (b) crystals grown in Acid-3 and Acid-4 gels against ICSD reference #242181 pattern. Broad peak at $2\theta \approx 12^\circ$ originates from the "low background" powder sample holder.

to compress and create enough space for nucleation and crystal growth.

Powder X-ray diffraction was employed to investigate the structure of formed crystals, with the patterns compared to reference data from the Inorganic Crystal Structure Database (ICSD) (Fig. 10).[38] From these data, it can be seen that almost all the crystals grown in ionogels contain impurities, especially the ones collected from Acid-1 and Acid-2 gels. Several strong and sharp peaks were recorded at around $2\theta \approx 9.5^\circ$, and most of the peaks were absent, especially in the pattern of crystals grown in Acid-1, suggesting that the formed crystals were not the ideal product. The matched peaks in the remained three pattern showed slight shifts of different extents (about 0.05–0.1° for crystals in Acid-2, 0.1° for crystals in Acid-3 and within 0.15° for crystals in Acid-4) to higher $2\theta$ values compare with reference, which indicated the change in lattice structure, potentially due to the inclusion of dopants during crystal growth.

From Fig. 10b, it can be seen that these two patterns were more consistent with the reference, especially the pattern of Acid-3 gel, the peaks were sharp and clear and matched well with the reference pattern, indicating good quality of the obtained crystals. In the pattern of Acid-4 gel though, there were outliers, but most peaks were still consistent with reference, confirmed that more favourable products were formed in Acid-3 and Acid-4 gels than in the previous two experiments. Considering the only difference between these ionogels was the IL added in synthesis, these results may suggest that crystals tend to have better growth in hexyl-imidazolium IL-based ionogels.

For the base-catalysed ionogels, when liquids were added to a U-tube, the reagents diffused rapidly inside the gel from one end to another through small cracks, unable to form the desired crystals, showing that these base-catalysed ionogels were not suitable for this application. Furthermore, unexpected reactions were observed between $BiI_3$ and the gel; upon the addition of $BiI_3$, a white-yellow solid formed immediately.

As can be seen in Fig. 11, a broad peak in the PXRD pattern is present at $2\theta \approx 24^\circ$, which is consistent with that previously observed in TEOS-based gels,[39,40] and silica nanoparticles produced in the presence of ammonia.[41] Such a peak is indicative of the amorphous nature of this solid and no crystalline substance was formed in this unexpected reaction. Whereas the two small peaks observed at $2\theta \approx 29^\circ$ and 31° could probably indicate the presence of bismuth(III) hydroxide. Bismuth(III) hydroxide $Bi(OH)_3$ is a yellowish-white solid that typically can be produced by adding alkali hydroxide solution to bismuth salts.[42] The PXRD pattern of $Bi(OH)_3$ prepared in basic solvent

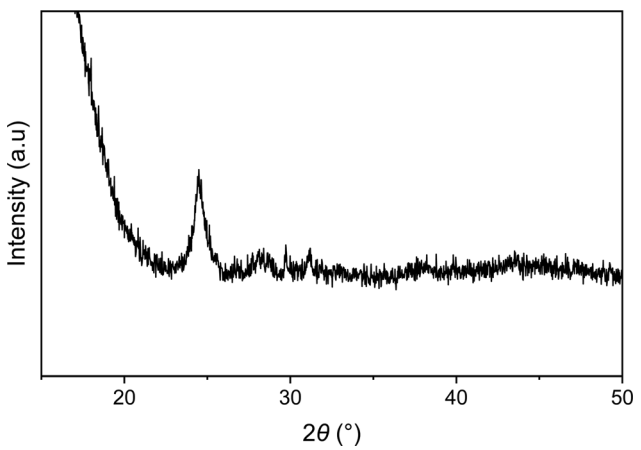


Fig. 11 PXRD pattern of the white–yellow solid obtained when $BiI_3$ reagent is added to the Base-1 gel, collected between 15–50° ($2\theta$). The broad peak at approximately 24° indicates the amorphous nature of the material.

(pH = 10) also shows similar peaks to this pattern.[43] With this evidence, it is suggested that the expected perovskite structure with MAI was not formed. Based on these results, it can be concluded that the desired crystalline product did not form during gel diffusion in the base-catalysed ionogel experiments.

### 3.2. Discussion

The main findings between acid- and base-catalysed ionogels are discussed in this section.

**3.2.1. Acid-catalysed ionogels.** Based on experimental data, in acid catalysis, transparent, homogeneous and hard gels were formed from all four precursors. According to previous studies, the particles and linear polymers formed at low pH bear no charge, when there is essentially no charge, the aggregation and flocculation will occur, particles collide and link with each other to form branched chains rather than large round particles.[19,32,44] These chain molecules in turn condense and crosslink with each other to form a 3D network, extend throughout the liquid medium, causing an increasing in viscosity, and eventually complete gelation, forming strong gels[19] and neck formation between particles as observed in TEM results. Additionally, in an acidic environment, the growth of particles is limited, the particles cease to grow after they have reached diameter of about 2–3 nm, which favours the interconnection between particles, and scatter less light, rendering highly transparent appearance of sols and gels.[19,26,32,44] The rate of aggregation also depends mainly on the number of particles per unit volume and less on their size, hence aggregation happens soon after polymeric particles are formed.[19]

Although the gels were initially strong and homogeneous, cracks appeared several hours after gelation, accompanied by ethanol leakage from the gel body. These observations suggest that reactions such as polymerisation, condensation, and depending on conditions, hydrolysis and esterification continued after gelation had occurred. Polymerisation continues between monomers and polymers due to the large number of SiOH groups present. An increase in the number of bonds decreases the flexibility of the network, thereby promoting syneresis and contraction of the gel, with liquid expelled from the pores as the network can only contract if the pore liquid is displaced.[45] In addition to these ongoing reactions, the capillary pressure exerted also influences the volume shrinkage and contraction in gels. Shrinkage depends on the maximum capillary pressure generated, in gels where the pores are small, high pressures are developed during drying, which causes the original network to collapse.[46–49] Based on Young's equation, the capillary pressure, $P_c$, could be calculated using eqn (1):[49,50]

$$P_c = -\frac{2\gamma_{LV}\cos(\theta)}{r_p} \quad (1)$$

where $\gamma_{LV}$ is the specific energy of the liquid–vapour interface, $\theta$ is the contact angle, and $r_p$ is the pore radius. Deshpande *et al.* found for a gel with an average pore radius of approximately 10 nm, the resulting capillary pressure is estimated to be approximately 140 atm (14.19 MPa) when water is used as the pore fluid.[48] As indicated by TEM and $N_2$ sorption analysis, acid-catalysed gels typically exhibit pores with diameters smaller than 20 nm, which means high capillary pressure could also develop inside the gels, causing shrinkage in structure.

The different ILs used in synthesis also influence gel properties. Based on experimental data, gels incorporated with different anions showed a much varied gelation time. Sols containing $BF_4^-$ anions could complete gelation within a few minutes. Traces of $F^-$ ions have a marked catalytic effect at low pH where it is mainly present as HF, conversion of sol to gel is also accelerated by $F^-$ ions at low pH.[32] According to literature, the catalytic activity of $BF_4^-$ anion is stronger than $PF_6^-$ anion and can act as a catalyst by itself.[1,51] Additionally, in the hydrolytic sol–gel process, $BF_4^-$ anion undergoes hydrolysis at room temperature in the presence of water and releases HF molecules,[7] which provides both an acid and a Lewis base,[2,7] a powerful catalyst for hydrolytic condensation of alkoxysilanes.[52] While $PF_6^-$ anions are more stable, their hydrolysis occurs to a much lesser extent under moderate conditions and is observed only under acidic (pH $<$ 3) and high-temperature conditions, which explains the less accelerated gelation time.[1,7]

**3.2.2. Base-catalysed ionogels.** Small variations in preparation conditions and precursor solutions can result in different final products. The structures of silicate polymers formed from alkoxides by the sol–gel process vary from weakly branched molecular networks to highly condensed particles depending on different pH values.[32] Unlike acid-catalysed ionogels, all the base-catalysed gels formed in this experiment were translucent, weak and visually crack-free. In an alkaline environment, sols are stabilised against gelling.[32] The majority of silanol groups at the surface are ionised by the hydroxyl anions present, resulting in a large surface charge on the silica particles preventing them from colliding and aggregating.[19,32] As stated above, when silica particles are not charged, they link together into branch chains to form 3D network regions. While at pH $>$ 7, particles remain aggregated and further cemented together as SEM and TEM results showed. In these cases, chain segments dissolve, and particle growth continues by Ostwald ripening without coalescence, eventually forming separated particles.[19,23,28] The low degree of coalescence results in weak gel strength, which is consistent with experimental results. In some extreme cases, the diameter of particles could be up to 35 nm and particles may precipitate prior to gelation. In this work, nanoparticles with diameters ranging from 3–5 nm and exhibiting a low degree of coalescence were obtained, owing to the ammonia-catalysed process, which minimises particle growth. The presence of $NH_4^+$ ions reduces the surface charge and allows particle collisions;[19,53] however, the influence is limited due to the small size of the cation.[23] The alkylimidazolium ILs may also helped to reduce aggregation and improve interphase interactions between particles.[13]

Experimental observations showed that viscosity remained low until the effective modifying agent PEG400 and ILs were added. The increase in viscosity suggests that particle aggregation was initially suppressed due to reduced collision frequency, while the catalytic activity of the ILs was also effective under base-catalysed conditions. The addition of PEG400

enhances mechanical properties improves interfacial bonding between particles, regulates sol structure to form homogeneous particle rings and subsequently drives gelation.[28] It is likely that the observed microstructure is primarily influenced by PEG400, rather than by the hydrolysis and polycondensation of TEOS in aqueous media. However, the overall effect is limited due to strong interparticle repulsion and low extent of coalescence, hence gels with low strength were formed under base-catalytic conditions here.

The opacity of the sols and gels also arises from the large particles remained in sols. As the particle size increases, the resulting transparency of gel is lost as more light is scattered by these particles.[49] Additionally, base-catalysis experiments do not undergo complete hydrolysis, the low conversion efficiency in low water base-catalysed TEOS left unhydrolysed TEOS monomers, which are also large enough to scatter light, resulting in high opacity.[32,44,49]

Another noticeable difference in appearance is that, unlike acid-catalysed gels, base-catalysed gels do not develop visible cracks in 2 weeks. According to eqn (1) and gas sorption analysis, base-catalysed gels have significantly larger pores, mainly mesopores between 15–35 nm and even potentially macropores. Comparing to acid-catalysed gels ($<20$ nm), the capillary pressure developed within base-catalysed gels tends to be much lower, hence less likely to develop cracks in the structure. Brinker *et al.* also stated that because the maximum capillary pressure is inversely related to the particle size and extent of aggregation, it is much lower for particulate gels than for the polymeric systems.[33]

However, since these gels are composed of discrete nanoparticles, as indicated by TEM results, they are naturally prone to liquid percolation through the spaces between packed particles, which aligns with observations when liquid reagents were added. Additionally, the high solvent ratio (1 TEOS:38 EtOH) increases the spacing between reacting species. The low oxide content in the diluted sol further enhances particle separation, resulting in larger voids within the particle packing structure,[47] further confirmed that base-catalysed gels are not ideal candidate for *in situ* crystal growth.

**3.2.3. Crystals.** The PXRD patterns revealed that all the crystals collected from the acid-catalysed ionogels contained impurities and exhibited peak shifts, indicating that other substances interfered with the crystal growth process. In acid-catalysed gels, the presence of small pores leads to extremely low permeability, causing the solid phase to compress and expel the liquids within. The remained liquids, water, ethanol, HCl and ILs may further interact with $BiI_3$ and MAI in the gel diffusion stage and subsequently alter the crystal formation process. NMR data visualised in Fig. S4–S7 and experimental observations suggest that HCl reacts with MAI, specifically with the methylamine component (likely forming methylammonium chloride ($CH_3NH_3Cl$), as shown in Fig. S7). These findings imply that the HCl catalyst not only modifies the gel structure but may also influence crystal growth through direct chemical interaction with the perovskite precursors.

# 4. Conclusions

In conclusion, these experiments demonstrate that the incorporation of ionic liquids in the sol–gel synthesis accelerates gelation times in acid and base catalysis systems, and ionogels were formed successfully in both systems. While the structures of formed acid- and base-catalysed ionogels align with existing literature, acid-catalysed ionogels tend to have an interconnected 3D structure and base-catalysed ionogels are more like weakly linked spherical nanoparticles.

Furthermore, experiments also confirmed the feasibility of growing $MA_3Bi_2I_9$ perovskite crystals in acid-catalysed ionogels. The strong network supported liquid diffusion inside the gel and the smaller pores (diameter $<20$ nm) allowed for a slower diffusion process, enabling nucleation. This method also shows potential for synthesising other $A_3B_2X_9$ perovskites, for instance, formamide and bromide perovskites in ionogel media. Additionally, these gels may also provide a good medium for the growth of crystals that have air-sensitive components (*e.g.*, tin(II)). However, there are still some drawbacks in these collected crystals. The grown crystals are relatively small, mostly around 2–5 mm, which may limit their applications. Additionally, the PXRD analysis showed that these crystals contain impurities in composition, with only one sample exhibiting no impurity peaks (crystals in Acid-3 gel, as shown in Fig. 10b). Slight shifts in peaks were observed in all four samples as well. The high capillary pressure resulting from small pores can develop cracks in the gels, allowing reagents to diffuse through these cracks and react fast, hence there is no effective nucleation for large crystals. Moreover, the confined ionic liquids may escape from the solid networks, interfering the crystal growth, causing impurities in the crystal structure.

However, the crystal growth was unsuccessful in base-catalysed ionogels. The base-catalysed ionogels are composed of monodispersed nanoparticles and contain much larger mesopores and even macropores in structure, enable rapid liquid percolation within gels, hence failed to grow crystals. Gels that are good candidates for crystal growth have a continuous structure in the solid phase.[54] Besides, the unexpected reaction between reagents and gel make them unsuitable material for growing $MA_3Bi_2I_9$ crystals.

Despite their small size, the obtained crystals are still good candidates for synthesising thin films for photodetectors and solar cells. By optimising the gel structure, it is possible to synthesise gels that are more beneficial for crystal growth and develop larger, more optimised crystals. Future work could focus on reducing syneresis in these gels and optimising the method of synthesising gels. This may involve adjusting the catalyst or solvent ratio in base catalysis to form a stronger, more crosslinked structure. And for the acid-catalysed gels, introducing post-gelation treatments such as aging and supercritical drying could potentially reduce shrinkage and remove remained solvents. These improvements could enhance the stability and applicability of ionogels in perovskite crystal growth.

 

## Author contributions

Yutong Shen: conceptualisation, formal analysis, investigation, methodology, software, validation, writing – original draft, and writing – review and editing; John D. Worth: formal analysis, software, visualisation, writing – original draft, and writing – reviewing and editing; Simon R. Hall: conceptualisation, methodology, supervision, writing – original draft, and writing – review and editing.

## Conflicts of interest

There are no conflicts to declare.

## Data availability

All data generated during the study are included in the article or its SI. The Fourier-transform infrared result, NMR spectra, and digital photograph of crystals are available in Supplementary Information. See DOI: **https://doi.org/10.1039/d5sm00608b**.

## Acknowledgements

Y. S. thanks the Hall Group and the University of Bristol Scholarship [U119281-108]. J. D. W. thanks the Engineering and Physical Science Research Council through the EPSRC Centre for Doctoral Training in Composites Science, Engineering and Manufacturing [EP/S021728/1]. The authors thank Dr Subash Sharma and Dr Lui Terry for their help in characterisation and with data analysis.

## Notes and references

1 L. Viau, M.-A. Néouze, C. Biolley, S. Volland, D. Brevet, P. Gaveau, P. Dieudonné, A. Galarneau and A. Vioux, *Chem. Mater.*, 2012, **24**, 3128–3134.
2 A. Karout and A. C. Pierre, *Catal. Commun.*, 2009, **10**, 359–361.
3 D. C. Green, S. Glatzel, A. M. Collins, A. J. Patil and S. R. Hall, *Adv. Mater.*, 2012, **24**, 5767–5772.
4 R. Tomaš, *Croat. Chem. Acta*, 2021, **94**(2), 83–94.
5 J. Fuller, A. C. Breda and R. T. Carlin, *J. Electrochem. Soc.*, 1997, **144**, L67.
6 A. K. Gupta, M. P. Singh, R. K. Singh and S. Chandra, *Dalton Trans.*, 2012, **41**, 6263–6271.
7 M. G. Freire, C. M. S. S. Neves, I. M. Marrucho, J. A. P. Coutinho and A. M. Fernandes, *J. Phys. Chem. A*, 2010, **114**, 3744–3749.
8 M. Tariq, P. A. S. Forte, M. F. C. Gomes, J. N. C. Lopes and L. P. N. Rebelo, *J. Chem. Thermodyn.*, 2009, **41**, 790–798.
9 N. W. Smith, J. Knowles, J. G. Albright and S. V. Dzyuba, *J. Mol. Liq.*, 2010, **157**, 83–87.
10 A. E. Danks, S. R. Hall and Z. Schnepp, *Mater. Horiz.*, 2016, **3**, 91–112.
11 R. K. Donato, M. Lavorgna, P. Musto, K. Z. Donato, A. Jager, P. Stepanek, H. S. Schrekker and L. Matejka, *J. Colloid Interface Sci.*, 2015, **447**, 77–84.
12 M. Wang, J. Hu and M. D. Dickey, *NPG Asia Mater.*, 2023, **15**, 66.
13 M. Perchacz, R. K. Donato, L. Seixas, A. Zhigunov, R. Konefal, M. Serkis-Rodzen and H. Benes, *ACS Appl. Mater. Interfaces*, 2017, **9**, 16474–16487.
14 M.-A. Néouze, J. Le Bideau and A. Vioux, *Prog. Solid State Chem.*, 2005, **33**, 217–222.
15 E. Andrzejewska, A. Marcinkowska and A. Zgrzeba, *Polimery*, 2017, **62**, 344–352.
16 A. R. Patel and A. Venkateswara Rao, *Bull. Mater. Sci.*, 1982, **4**, 527–548.
17 N. I. Selivanov, A. O. Murzin, V. I. Yudin, Y. V. Kapitonov and A. V. Emeline, *CrystEngComm*, 2022, **24**, 2976–2981.
18 Y.-T. Huang, S. R. Kavanagh, D. O. Scanlon, A. Walsh and R. L. Z. Hoye, *Nanotechnology*, 2021, **32**, 132004.
19 R. K. Iler, *The Chemistry of Silica: Solubility, Polymerization, Colloid and Surface Properties, and Biochemistry*, Wiley, New York, 1979.
20 C. J. Brinker and G. W. Scherer, in *Sol-Gel Science*, ed C. J. Brinker and G. W. Scherer, Academic Press, San Diego, 1990, ch. 3, pp. 96–233.
21 S. Dai, Y. H. Ju, H. J. Gao, J. S. Lin, S. J. Pennycook and C. E. Barnes, *Chem. Commun.*, 2000, 243–244.
22 F. Shi and Y. Deng, *Spectrochim. Acta, Part A*, 2005, **62**, 239–244.
23 A. Rodrigues, B. Sena da Fonseca, A. P. Ferreira Pinto, S. Piçarra and M. F. Montemor, *New J. Chem.*, 2021, **45**, 3833–3847.
24 O. Malay, I. Yilgor and Y. Z. Menceloglu, *J. Sol-Gel Sci. Technol.*, 2013, **67**, 351–361.
25 K. Donato, L. Matějka, R. Mauler and R. Donato, *Colloids Interfaces*, 2017, **1**(5), DOI: **10.3390/colloids1010005**.
26 L. C. Klein, in *Encyclopedia of Modern Optics*, ed R. D. Guenther, Elsevier, Amsterdam, 2005, pp. 16–21.
27 T. A. Saleh, in *Interface Science and Technology*, ed T. A. Saleh, Elsevier, Amsterdam, 2022, vol. 34, pp. 127–165.
28 Y. Xiang, X. Li, A. Du, S. Wu, J. Shen and B. Zhou, *J. Coat. Technol. Res.*, 2016, **14**, 447–454.
29 S. Brunauer, P. H. Emmett and E. Teller, *J. Am. Chem. Soc.*, 1938, **60**, 309–319.
30 J. P. Olivier, *J. Porous Mater.*, 1995, **2**, 9–17.
31 Z. V. Faustova and Y. G. Slizhov, *Inorg. Mater.*, 2017, **53**, 287–291.
32 H. E. Bergna and W. O. Roberts, *Colloidal Silica: Fundamentals and Applications*, Taylor & Francis, Boca Raton, 2005.
33 C. J. Brinker and G. W. Scherer, in *Sol-Gel Science*, ed C. J. Brinker and G. W. Scherer, Academic Press, San Diego, 1990, ch. 9, pp. 514–615.
34 M. Thommes, K. Kaneko, A. V. Neimark, J. P. Olivier, F. Rodriguez-Reinoso, J. Rouquerol and K. S. W. Sing, *Pure Appl. Chem.*, 2015, **87**, 1051–1069.
35 S. J. Gregg and K. S. W. Sing, *Adsorption, Surface Area, and Porosity*, Academic Press, London, 1982.

36 E. Framery and P. H. Mutin, *J. Sol-Gel Sci. Technol.*, 2002, **24**, 191–195.
37 R. Babu, S. Bhandary, D. Chopra and S. P. Singh, *Chem. – Eur. J.*, 2020, **26**, 10519–10527.
38 M. E. Kamminga, A. Stroppa, S. Picozzi, M. Chislov, I. A. Zvereva, J. Baas, A. Meetsma, G. R. Blake and T. T. M. Palstra, *Inorg. Chem.*, 2017, **56**, 33–41.
39 J. R. Martínez, S. Palomares-Sánchez, G. Ortega-Zarzosa, F. Ruiz and Y. Chumakov, *Mater. Lett.*, 2006, **60**, 3526–3529.
40 R. K. Satvekar, M. R. Phadatare, V. A. Karande, R. N. Patil, B. M. Tiwale and S. H. Pawar, *Int. J. Basic Appl. Sci.*, 2012, **1**, 468–476.
41 G. Ren, H. Su and S. Wang, *J. Sol-Gel Sci. Technol.*, 2020, **96**, 108–120.
42 E. Wiberg, N. Wiberg and A. F. Holleman, *Inorganic Chemistry*, Elsevier, Amsterdam, 2001.
43 S. Liu, G. Ren, X. Gao, Z. Li, L. Wang and X. Meng, *Chem. Commun.*, 2022, **58**, 8198–8201.
44 L. C. Klein and G. J. Garvey, *MRS Online Proc. Libr.*, 2011, **32**, 33.
45 G. W. Scherer, *J. Non-Cryst. Solids*, 1988, **100**, 77–92.
46 D. M. Smith, G. W. Scherer and J. M. Anderson, *J. Non-Cryst. Solids*, 1995, **188**, 191–206.
47 A. Venkateswara Rao and S. D. Bhagat, *Solid State Sci.*, 2004, **6**, 945–952.
48 R. Deshpande, D.-W. Hua, D. M. Smith and C. J. Brinker, *J. Non-Cryst. Solids*, 1992, **144**, 32–44.
49 P. J. Davis, C. J. Brinker, D. M. Smith and R. A. Assink, *J. Non-Cryst. Solids*, 1992, **142**, 197–207.
50 C. J. Brinker and G. W. Scherer, in *Sol-Gel Science*, ed C. J. Brinker and G. W. Scherer, Academic Press, San Diego, 1990, ch. 7, pp. 406–451.
51 L. Y. Guo, J. Shi, J. H. He, J. Y. Huang and P. C. Huang, *Appl. Mech. Mater.*, 2015, **727–728**, 34–37.
52 A. Okabe, T. Fukushima, K. Ariga, M. Niki and T. Aida, *J. Am. Chem. Soc.*, 2004, **126**, 9013–9016.
53 S. Nandy, D. Kundu and M. K. Naskar, *J. Sol-Gel Sci. Technol.*, 2014, **72**, 49–55.
54 O. Velásquez-González, C. Campos-Escamilla, A. Flores-Ibarra, N. Esturau-Escofet, R. Arreguin-Espinosa, V. Stojanoff, M. Cuéllar-Cruz and A. Moreno, *Crystals*, 2019, **9**, 443.

 